Freshwater content variability in the Arctic Ocean

S. Häkkinen
NASA Goddard Space Flight Center, Greenbelt, Maryland, USA

A. Proshutinsky
Woods Hole Oceanographic Institution, Woods Hole, Massachusetts, USA

Received 29 April 2003; revised 9 December 2003; accepted 12 January 2004; published 31 March 2004.

[1] Arctic Ocean model simulations have revealed that the Arctic Ocean has a basin-wide oscillation with cyclonic and anticyclonic circulation anomalies (Arctic Ocean Oscillation (AOO)) that has a prominent decadal variability [*Proshutinsky and Johnson*, 1997]. This study explores how the simulated AOO affects the Arctic Ocean stratification and its relationship to the sea ice cover variations. The simulation uses the Princeton Ocean Model coupled to sea ice [*Häkkinen and Mellor*, 1992; *Häkkinen*, 1999]. The surface forcing is based on National Centers for Environmental Prediction/National Center for Atmospheric Research Reanalysis and its climatology, of which the latter is used to force the model spin-up phase. Our focus is to investigate the competition between ocean dynamics and ice formation/melt on the Arctic basin-wide freshwater balance. We find that changes in the Atlantic water inflow can explain almost all of the simulated freshwater anomalies in the main Arctic basin. The Atlantic water inflow anomalies are an essential part of AOO, which is the wind driven barotropic response to the Arctic Oscillation (AO). The baroclinic response to AO, such as Ekman pumping in the Beaufort Gyre, and ice melt/freeze anomalies in response to AO are less significant considering the whole Arctic freshwater balance. *INDEX TERMS:* 4207 Oceanography: General: Arctic and Antarctic oceanography; 4215 Oceanography: General: Climate and interannual variability (3309); 4255 Oceanography: General: Numerical modeling; 4283 Oceanography: General: Water masses; *KEYWORDS:* fresh water, Arctic, variability

Citation: Häkkinen, S., and A. Proshutinsky (2004), Freshwater content variability in the Arctic Ocean, *J. Geophys. Res.*, *109*, C03051, doi:10.1029/2003JC001940.

1. Introduction

[2] Influence of the Arctic Ocean and its sea ice cover downstream in the Atlantic is of interest in the climate community because of its mobile and large freshwater content. It has been recognized for several years that the ice export through Fram Strait is highly variable both from model simulations [*Walsh et al.*, 1985; *Häkkinen*, 1993; *Häkkinen and Geiger*, 2000] and from observations [*Vinje*, 2001] and that it could be of major influence on the North Atlantic thermohaline structure and overturning [*Dickson et al.*, 1988, 1996; *Mauritzen and Häkkinen*, 1997; *Holland et al.*, 2001]. The changes in the liquid freshwater content of the Arctic have been left largely untouched except for the discussion provided by *Proshutinsky et al.* [2002]. They propose that the storage changes of fresh water in the anticyclonic Beaufort Gyre can potentially be much larger than river runoff changes and ice export events. The changes in the fresh water are tied to the decadal mode of ocean circulation variations, the Arctic Ocean Oscillation (AOO) [*Proshutinsky and Johnson*, 1997], which is defined on the basis of sea surface height in a barotropic ocean model. The basic premise of the Proshutinsky et al. hypothesis is that the Ekman transport will act to increase the freshwater content in the Beaufort Gyre when the AOO mode is anticyclonic and to decrease it for cyclonic AOO. Also they show a comparison of the freshwater content as estimated from a model sea surface height with a simulated total sea ice volume which suggests that the oceanic freshwater and sea ice volume anomalies [from *Hilmer and Lemke*, 2001] are nearly in phase (except perhaps before 1970). This latter result should not be surprising if AOO and its atmospheric forcing affect both the ocean freshwater and sea ice volume anomalies, but it is notable that according to their computation, the in-phase relationship of those volume anomalies makes the Arctic ocean and ice freshwater storage changes nearly 3 times as large as the annual climatological river runoff of 3800 km^3.

[3] Here we undertake anew this hypothesis based on the coupled ice-ocean model hindcast for the period 1951–2001. The model uses National Centers for Environmental Prediction/National Center for Atmospheric Research (NCEP/NCAR) Reanalysis data for surface forcing anomalies (section 2). With the inclusion of ice volume, ice growth/melt rates and the dynamic ocean we will analyze the influence of these components on the basin-wide salt content anomalies to test the validity of the Proshutinsky et al. hypothesis. These various mechanisms are presented in section 3. The evolution of the freshwater anomalies in

Copyright 2004 by the American Geophysical Union.
0148-0227/04/2003JC001940

ocean and ice is discussed in sections 4.1 and 4.2. The relative importance of various mechanisms for the anomalies is discussed in section 4.3. We omit variability in river runoff, precipitation-evaporation and Bering Strait inflow in order to concentrate to dynamic and thermodynamic processes. The discussion of heat content anomalies associated with AOO is also omitted because they were investigated at length by *Häkkinen and Geiger* [2000].

2. Ocean Model Description and Its Forcing

2.1. Ocean Model

[4] The ocean model is hydrostatic and Boussinesq and uses the sigma coordinate system as described by *Blumberg and Mellor* [1987] with a modified scalar advection scheme to avoid overshooting at sharp fronts [*Mauritzen and Häkkinen*, 1997]. The 2.5 level turbulence closure scheme of *Mellor and Yamada* [1982] is used to determine the vertical mixing coefficients for momentum and scalar variables. The dynamic-thermodynamic ice model is coupled to the ocean model via interfacial stresses and via salinity and heat fluxes through the ice-water interface. The ice model uses a generalized viscous rheology as discussed by *Häkkinen and Mellor* [1992].

[5] The coupled ice-ocean model extends from the Bering Strait to 15°S with resolution of 7/10° in 'longitude', 9/10° in 'latitude' (in a rotated coordinate system with equator at 30°W and the pole at (120°W, 0°N). There are a total of 20 sigma levels in the vertical with higher resolution near the surface. To minimize the inaccuracies in the computation of the pressure gradient, the topography (derived from the TerrainBase Global DTM database with 5′x5′ resolution) is smoothed heavily. However, the Nordic sills were retained with their (real) depth of 650 m at Denmark Strait and of 1100 m at the Faeroe-Shetland Channel.

[6] The initialization of a 20 year quasi-equilibrium run was started from the annual average hydrographic climatology of *World Ocean Atlas 1998*. The vertically averaged transports at oceanic lateral boundaries were specified to be 0.8 Sv through the Bering Strait, and 0.8 Sv out at 15°S. At the northern and southern boundary the salinities and temperatures are relaxed to monthly climatological values. Restoring of T and S is also used at the Mediterranean outflow point. The water masses in the upper ocean and just below the permanent thermocline (e.g., Labrador Seawater) have timescales of a decade (Rossby wave transmission in the model midlatitudes is 6 years across the basin). Thus the decadal variability and deep ocean timescales are rather well separated and one can consider the decadal variability superimposed on the slower deep ocean variability. The same model results concerning the meridional heat transport, overturning and their atmospheric forcing are discussed by *Häkkinen* [1999, 2000, 2001].

2.2. Model Forcing

[7] The model is forced with monthly climatological data computed from the NCEP/NCAR Reanalysis for the first 20 years, after which monthly varying Reanalysis fields (wind stress, wind speed, air temperature and specific humidity) are phased in 4 years, first appending COADS monthly anomalies [*da Silva et al.*, 1994] to the Reanalysis climatology from 1945 to 1947 and then blending COADS and Reanalysis data during 1948. From 1949 to 2002 the forcing is solely NCEP/NCAR Reanalysis data. The simulated data are stored as monthly averages, and only the years 1951 through 2002 are used for the presented analysis.

[8] The cloudiness and the precipitation minus evaporation (P-E) field and river runoff are climatological throughout simulations (see 2.3 for further considerations). The surface boundary condition for salinity uses virtual flux of salt, i.e., (P-E) * SSS (SSS = sea surface salinity) modified by the brine/meltwater flux in the ice covered ocean. River runoff is also treated as a virtual flux of salt. For the heat exchange the bulk formulation is adopted where the heat fluxes are a function of the oceanic surface quantities. Heat exchange coefficient of 1.3×10^{-3} is used regardless of air-ocean stability conditions. The surface mixing ratio is computed from the model sea surface temperature (SST) with 98% saturation. The model SST is also used in the upward long-wave radiation.

2.3. Omissions From the Numerical Simulation With Respect to the Freshwater Balance

[9] At the outset our goal is to concentrate on dynamic and thermodynamic processes influencing the Arctic freshwater content, however, the omitted sources of variability (P-E, rivers and Bering inflow) in the numerical model are in need of a few comments. In case of the year-to-year variability of P-E, we can estimate the net freshwater anomalies on the basis of the NCEP/NCAR Reanalysis. The annual P-E anomalies in the Arctic Basin referenced to the mean of 1948 to 2001 are shown in Figure 1. The anomalies are mostly limited to ±200 km^3/yr with the exception of the early period when data may have been even less reliable. These values represent about 10% of the net annual precipitation over the Arctic.

[10] The Bering Strait throughflow variability is also excluded by the specification of the flux value to 0.8Sv which is regulated by the secular sea level gradient between the Pacific and the Atlantic [*Coachman et al.*, 1975; *Coachman and Aagaard*, 1988]. A flux of 0.8Sv of Pacific waters amounts to 1670 km^3 of freshwater input per year (the Bering inflow salinity 32.5 ppt, and the Arctic reference salinity is 34.8 ppt). For example a change of 0.1 Sv in the inflow over a year would mean about 200 km^3 change in the freshwater input. The inflow data estimated from a barotropic model of *Proshutinsky and Johnson* [1997] (and extended to 2002 using NCEP/NCAR Reanalysis data) in Figure 1 shows that the Bering inflow freshwater anomalies fall in the range of ±200 km^3. These values represent the wind driven contribution to the inflow.

[11] Variability in the river runoff is also excluded from the simulation. A total of about 3800 km^3 of runoff flows to the main basin in the model simulation. The variations in the river runoff from the observations [*Shiklomanov et al.*, 2000] (Figure 1a) have a range of ±600 km^3, but the average year-to-year changes are about ±200 km^3. In summary, the P-E, runoff, and the Bering inflow changes have to be in phase to be able make a significant contribution to the basin-wide freshwater anomalies. The largest total anomalies from these sources in Figure 1 amount to peak-to-peak variation of 1300 km^3. However, the range of volume

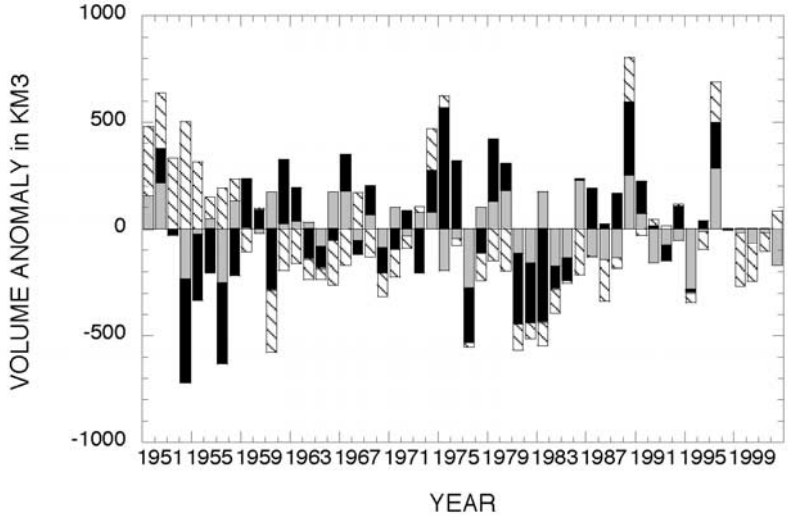

Figure 1. The stacked columns of interannual anomalies of P-E (dashed) from NCEP/NCAR Reanalysis, river runoff (black) to the Arctic Ocean from *Shiklomanov et al.* [2000], and the freshwater impact from Bering inflow (shaded) (referenced to 34.8 ppt) from *Proshutinsky and Johnson*'s [1997] (updated) model. Units are in km^3.

changes are small compared to the values we find in the following as the basin average anomalies.

3. Mechanisms for the Basin-Wide Freshwater/Salt Anomalies

3.1. Freshwater Accumulation and Release Mechanism

[12] A mechanism for the accumulation and release of fresh water in the Arctic Ocean was formulated by *Proshutinsky et al.* [2002]. Their hypothesis centers on the Beaufort Gyre, and the temporal variability of its freshwater content. The Canadian Basin contains about 45,000 km^3 of fresh water calculated relative to the salinity 34.80 by *Aagaard and Carmack* [1989], which is 10–15 times larger than the total annual river runoff to the Arctic Ocean, and at least two times larger than the amount of fresh water stored in the sea ice. The proposed mechanism works such that the Beaufort Gyre accumulates freshwater under anticyclonic wind forcing due to Ekman pumping and releases it when this wind is weaker or cyclonic. A key feature is accumulation and release of fresh water from the layers deeper than 75 m, which should determine if the mechanism is active in numerical simulations.

3.2. Freshwater Content Anomalies Due to Sea Ice Melt and Growth

[13] Freshwater content anomalies are associated with both dynamic and thermodynamic processes in the atmosphere and ocean. In terms of two circulation regimes, the freshwater content in the surface layer of the ocean should increase during a cyclonic circulation regime when sea ice melts more rapidly and ocean accumulates more heat during summer than during a short summer of an anticyclonic circulation regime [*Polyakov et al.*, 1999; *Maslowski et al.*, 2000]. During an anticyclonic circulation regime, or negative phase of the Arctic Oscillation [*Thompson and Wallace*, 1998], the Arctic Ocean should produce positive salinity anomalies because of lower air temperature and higher rates of sea ice production, and shorter period of sea ice melt season [*Polyakov et al.*, 1999]. Where, however, are these anomalies generated and what are the pathways of these anomalies in the Arctic Ocean? *Häkkinen* [1993] showed that large salinity anomalies were formed along the coast both east and west from the Bering Strait as a result of anomalous sea ice growth. Furthermore the same study showed that these anomalies propagated anticyclonically toward the Fram Strait, and some of the anomaly events exited to the GIN Seas. Recently, *Goosse et al.* [2002] found similar salinity anomalies associated with the sea ice growth anomalies in the Arctic Ocean. The downstream effect of these positive/negative salinity anomalies are shown by *Goosse et al.* [2002] to support/suppress deep water formation and overturning circulation.

3.3. Anomalous Advection of the Atlantic Waters to the Arctic Ocean

[14] A possible competitor to the processes discussed in 3.1 and 3.2 is the variability of inflow of Atlantic Water (AW) to the Arctic Ocean. At least two factors play a significant role here: the volume flux and the salinity of the Atlantic Water penetrating the Arctic Ocean. Unfortunately, these parameters of the AW are not well established observationally. It is possible that the variability of freshwater content (accumulation or release) in the Beaufort Gyre is compensated by the variability of the AW inflow to the Arctic Ocean. Both processes are regulated by AOO (see *Proshutinsky et al.* [2002] for the Beaufort Gyre and *Häkkinen and Geiger* [2000] for the variability of AW inflow to the Arctic Ocean). This topic will be revisited in section 4.2.

4. Results

4.1. Basin Average Salinity/Freshwater and Sea Ice Volume Variability

[15] Definition of the Arctic Basin in the following computations includes also the eastern part of the Barents Sea and Kara Sea because of the grid orientation (the boundary is shown in Figure 6a). The shallow Barents

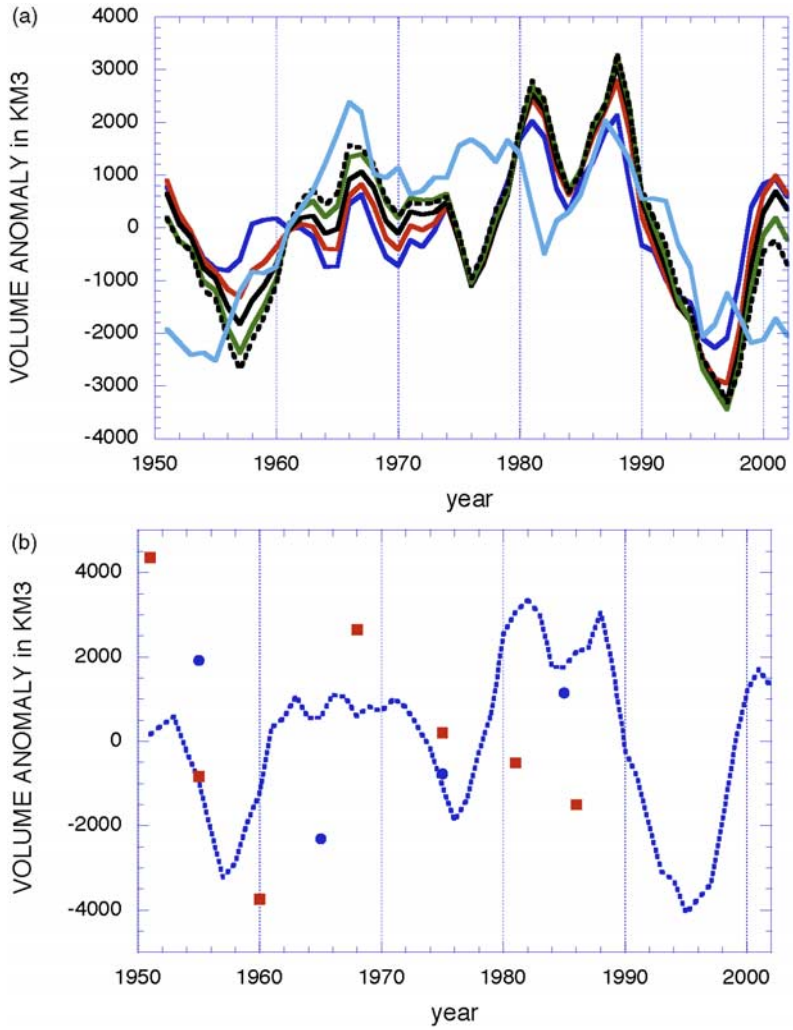

Figure 2. (a) The simulated values of freshwater anomalies as referenced to the climatology in the top 100, 200, 300, 500, and 1000 m layers and the ice volume anomaly (thick aqua blue line). All units are in km^3, and all data are detrended linearly. (b) The observed (dots and squares) and simulated (dashed) freshwater anomaly in the top 300 m for the whole of the Arctic Ocean excluding shelves shallower than 300 m. The (blue) dots refer to decadal averages from the AARI data, and the (red) squares refer to freshwater anomaly for the anticyclonic (1950–1952, 1958–1963, 1972–1979, and 1984–1988) and cyclonic (1953–1957, 1964–1971, and 1980–1983) regimes. All units in km^3.

and Kara Seas represent only a small fraction of the main Arctic volume, thus their salt freshwater variations should not weigh heavily in the estimates for the Arctic Ocean as a whole. To display the magnitude and variability of the simulated Arctic Ocean freshwater anomalies, we start from computing the basin average salinity and the corresponding freshwater anomaly referenced to the monthly climatology. The freshwater anomaly (v) corresponding to salinity S is defined simply as

$$v = V(So - S)/So; \quad (1)$$

where V is the volume of the given layer in the basin, and So is its climatological salinity. The annual freshwater anomaly time series for layer depths of 100, 200, 300, 500, and 1000 m and the sea ice volume anomaly are shown in Figure 2a. The annually averaged oceanic freshwater anomalies range from −3500 km^3 to +3500 km^3 (about ±40 cm if distributed evenly over the Arctic Basin), and the sea ice volume anomalies range from −2500 km^3 to +2500 km^3. The standard deviations for the 100, 200, 300, 500, and 1000 m layers and sea ice volume are 992, 1247, 1364, 1490, 1527, and 1454 km^3, respectively. For most part the same oceanic freshwater anomalies are imprinted to all of the depths shown, except at the beginning when the model may be still adjusting to the variable forcing. It appears that the upper ocean freshwater anomalies and sea ice volume anomalies are not in phase until during the last 15 years of the record. There is no a priori reason that they should be in phase because wind driven and thermodynamic effects, for example, as a response to AO, can project differently on the ocean and sea ice.

[16] The observations of the Arctic Ocean salinity are limited, but data collected by the Russian researchers have been made available to us by L. Timokhov from the Arctic-Antarctic Research Institute (St. Petersburg, Russia). The available data from 1950s to the 1980s (as salinity averaged

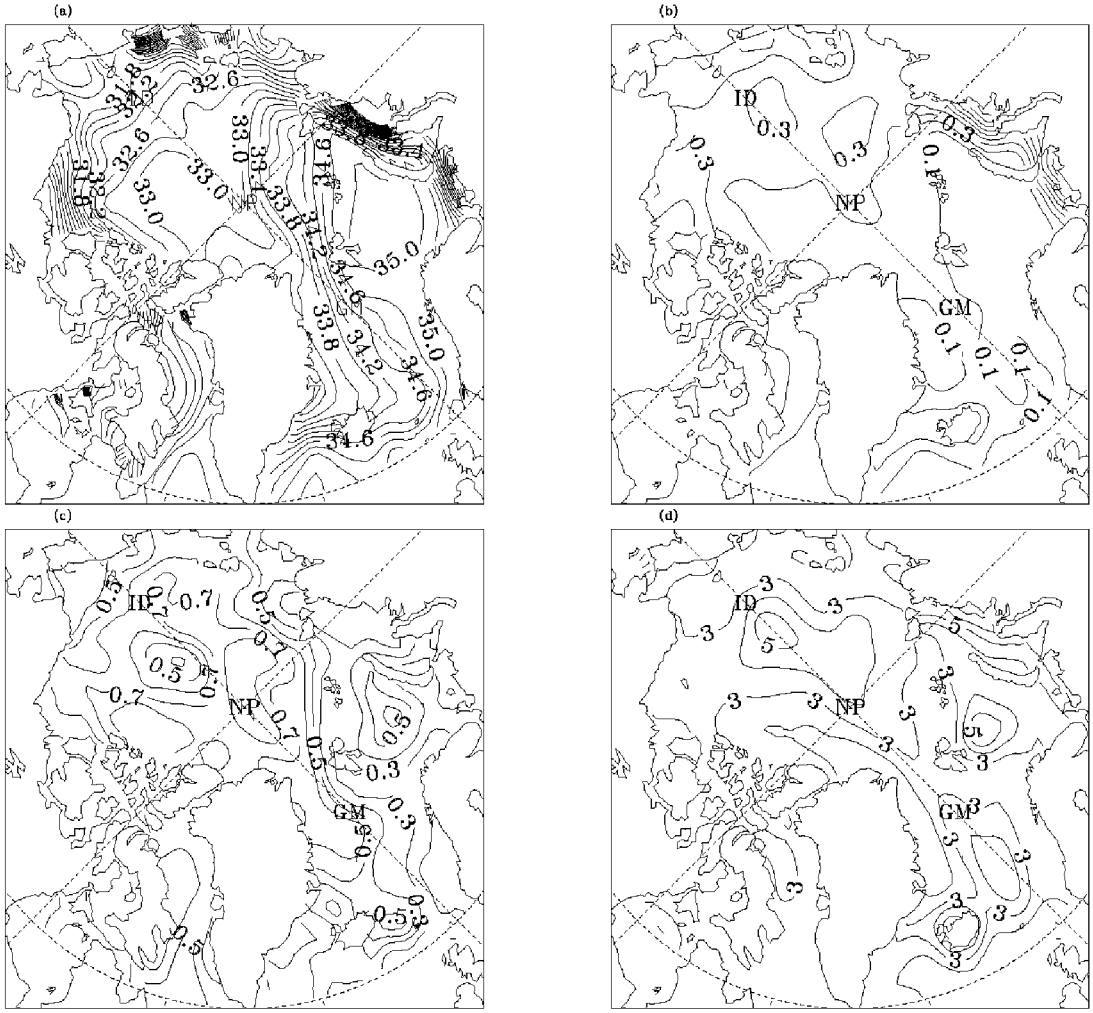

Figure 3. (a) The simulated 100 m average salinity (in ppt), (b) its standard deviation (computed from monthly anomalies) (in ppt), and (c) the fraction of the variance concentrated in longer timescales than 5 years (nondim.). (d) The standard deviation of the simulated sea surface height in cm.

over the top 300 m) have been compiled to a basin-wide freshwater volume anomaly in two different ways: (1) based on the years of cyclonic and anticyclonic regime years since 1950s or (2) by decades. The data coverage has been variable through the decades with the 1950s and 1970s having samples from most of the central basins, the 1960s had observations mainly on the Siberian side of the central basins, and a shift of observations closer to the Siberian coast occurred in 1980s. The Siberian shelf areas were sampled 'well' during the 1970s and 1980s, but for uniformity, the Siberian Shelf areas are excluded in the data points shown in Figure 2b which are shallower than 300 m. These freshwater anomalies are shown together with the model time series of 300 m freshwater content excluding Siberian shelves. Both the observations and the model agree that in the early 1950s were more fresh than the mid-1950s. Even in the 1960 and 1970s the model curve and the limited observations agree, but in the 1980s there is a discrepancy between the observed data (the regime average in particular) and the model. The spatial distribution of observations varied significantly from decade to decade, which can lead to biases in the regime averages and decadal averages as seen from the Figure 2b.

[17] To review the general spatial properties of the salinity variability, we show here only the upper 100 m average salinity field because it describes the spatial distribution of depth averaged salinity variations in the upper Arctic Ocean down to 1000 m. The simulation mean salinity field of the upper 100 m and its (nonseasonal) standard deviation are shown in Figures 3a–3b. Each salinity change of 0.2 ppt over 100 m corresponds to freshwater content change of about 60 cm (at the coastal depths 50 m, the freshwater change is about 30 cm). The high variance pattern circles the basin along the Transpolar Drift Stream and the coastal areas of the Canada Basin back toward the Siberian side. To highlight further the low-frequency variability of the salinity variability, the salinity time series is normalized at each grid point and then low-pass filtered by removing variability less than 5 years. The resulting field (Figure 3c) is the fraction of the standard deviation (in Figure 3b) that is associated with longer term variability. The low-frequency part of the standard deviation encircles the whole Arctic basin with a minimum in the central Canada Basin. The freshwater content anomalies are also imprinted to the sea surface height standard deviation

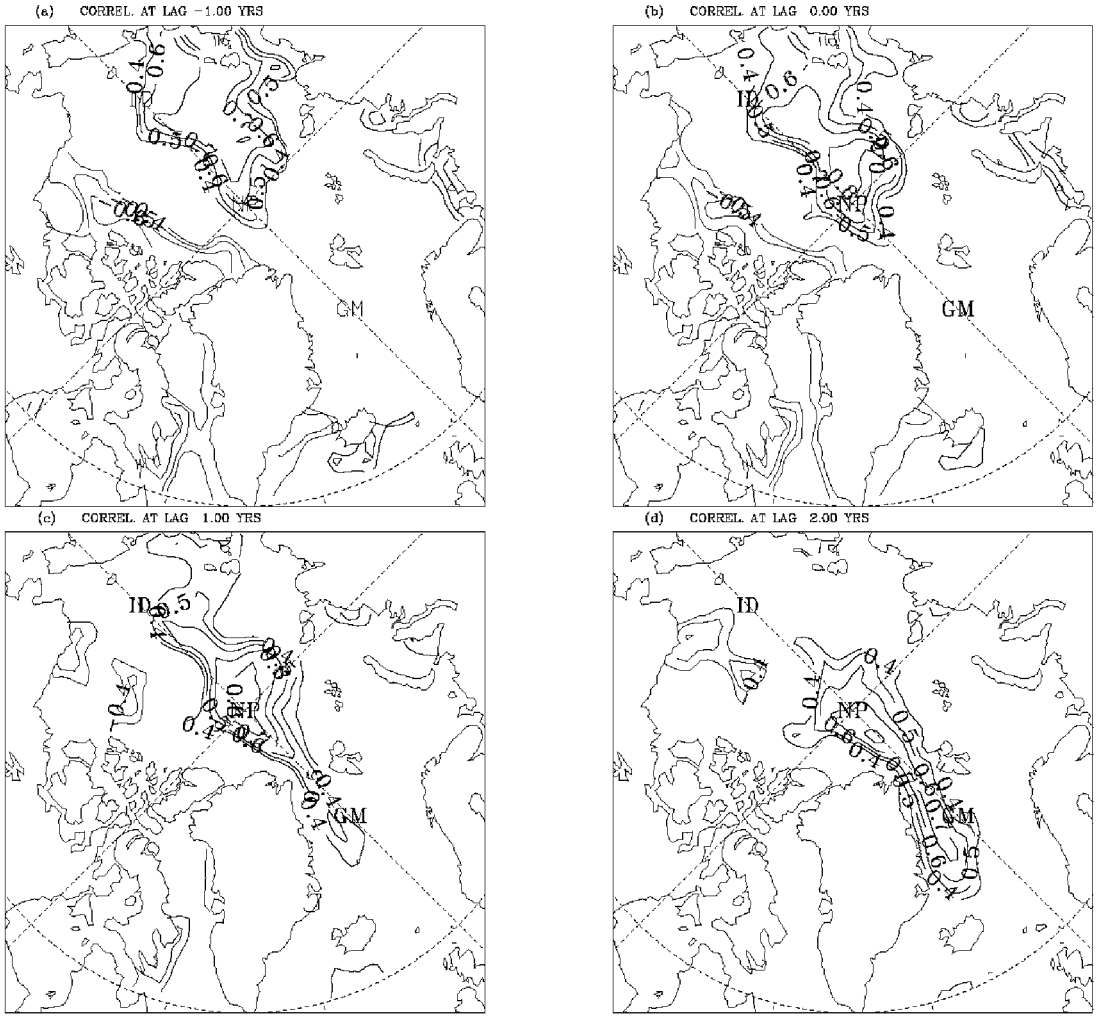

Figure 4. The correlation of the basin average 100 m salinity anomaly with its individual grid point anomalies at lags (a) −1, (b) 0, (c) 1, and (d) 2 years.

(Figure 3d) with overlapping high variance regions, but only in the main Arctic. In Barents and GIN Seas the spatial distribution of variance for SSH and the upper ocean salinity differ considerably. Heat content variability and the barotropic wind driven response have to contribute to the difference in the SSH variability in those regions.

[18] Once salinity (=freshwater) anomalies are formed, they can be traced for long periods and long distances because the local surface salt/freshwater fluxes are usually too small compared to the advection of salt to damp out the anomalies. Using the basin-averaged salinity time series to correlate with its own spatially varying field can give clues where the salinity (=freshwater anomalies) form, and their lagged correlations can indicate the general movement of the anomalies. Here we show the correlations for the 100 m depth layer where its basin average is correlated with the values in the individual grid points (Figure 4) for lags −1, 0, 1, and 2 years. The correlation fields at lags −1 and 0 years show that there are two centers of activity: The East Siberian Shelf (extending to the Makarov Basin) and the coastal sea along the Canadian Archipelago. Coincidentally these areas have been implicated as the zones where the impact of AO is the most apparent in the sea ice velocity field (examples of the latter are shown, for example, by *Häkkinen and Geiger* [2000] from a model study and by *Rigor et al.* [2002] from Arctic Drifting Buoys). The subsequent evolution of the correlation fields shows that these anomalies from the East Siberian side can be tracked within 2 years into the Greenland Sea. This suggests that the sea ice related freshwater anomalies have a short residence time in the Arctic particularly the ones initiated in the East Siberian Shelf. Furthermore, the correlations suggest that some of the anomalies remain inside the Arctic and move anticyclonically with the mean field toward the Canada Basin. Meanwhile the anomalies of the opposite sign along the Canadian Archipelago move toward the Siberian shelves. This behavior of salinity anomalies moving around the Arctic Basin and partially exiting at the Fram Strait was noted already in the study by *Häkkinen* [1993] which covered much shorter simulation record.

[19] The 100 m salinity anomalies appear to exit the Arctic within a few years which timescale is in good agreement with the observations for the near-surface water masses in the Arctic. On the basis of tracer observations *Ekwurzel et al.* [2001] estimated that the residence time of the top 50 m is about 2 years, increasing to about 6 years at 100 m depth depending on location.

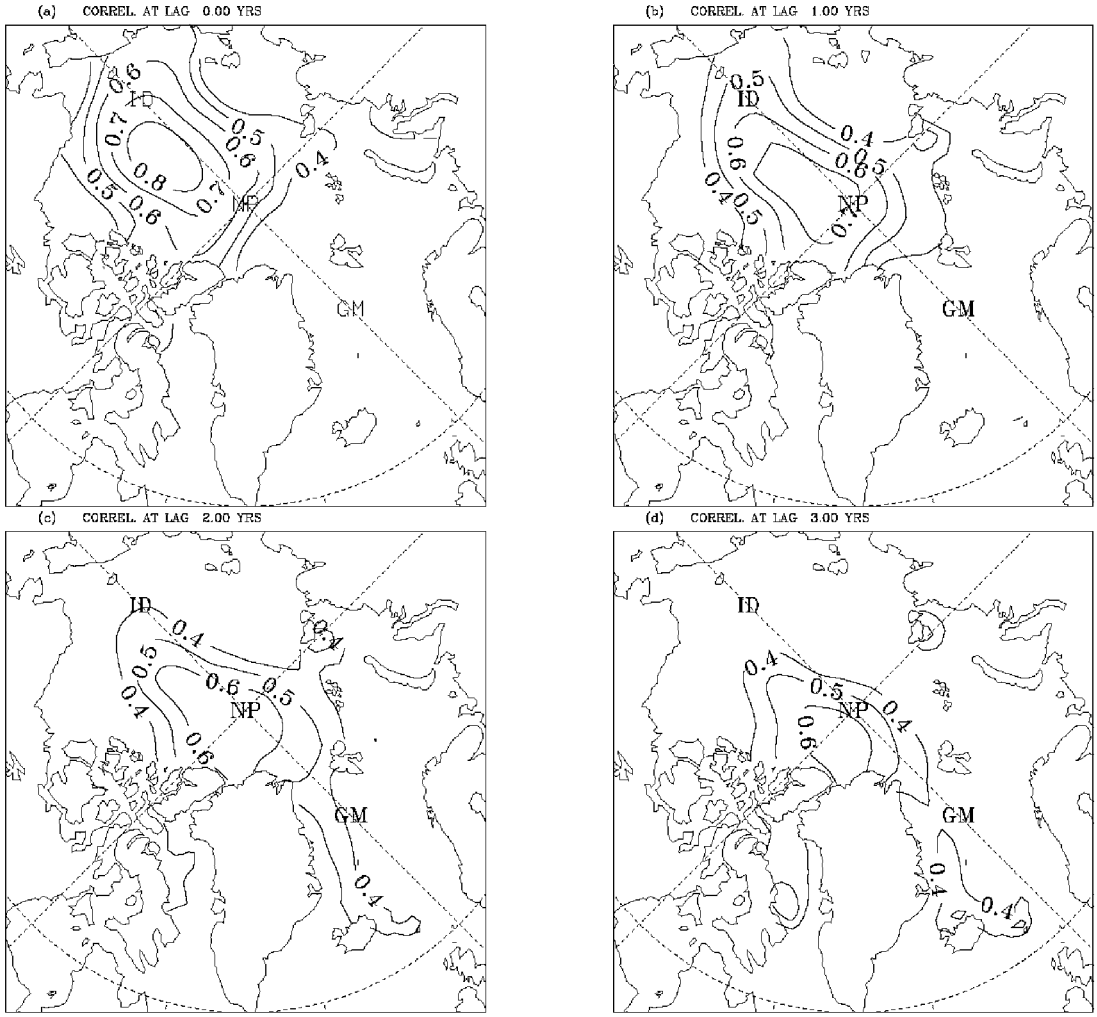

Figure 5. The correlation of the basin average sea ice volume anomaly with its individual grid point anomalies at lags (a) 0, (b) 1, (c) 2, and (d) 3 years.

[20] It was pointed out earlier that the basin average salinity and ice volume anomalies are not necessarily impacted similarly by the same atmospheric forcing such as to create two time series of high correlation. This is demonstrated by correlation fields between the basin average sea ice volume and the sea ice thickness field (Figure 5), correlations are shown at lags −1, 0, 1 and 2 years. The largest contribution to the basin average volume change comes from the central Canada Basin where the highest correlations do not overlap the highest-correlation region in Figure 4a. The balance between ice advection, internal ice rheology and the thermodynamic forcing determines where ice can thicken. As seen these areas do not need to coincide with areas of the largest salinity anomalies. The evolution of correlations suggests that eventually part of the ice volume anomalies exit through the Fram Strait.

4.2. Leading Modes of Variability for Circulation and Salinity

[21] A good index for the AOO is the principal component (PC) of the first EOF mode for the vertically averaged transport stream function. Originally, *Proshutinsky and Johnson* [1997] used gradient of sea surface height (SSH) variability from a barotropic ocean model to define AOO. Here we choose the stream function PC1 (but with opposite sign) to represent AOO because the first stream function EOF mode contains a large portion (here 71.5%) of the variance as already found by *Häkkinen and Geiger* [2000]. The first mode describes circulation changes which occur in unison in all of the Arctic and GIN Seas with secondary enhancements in the Canada, Eurasia and Norwegian Sea basins. In the following the stream function PC1 (PSI PC1) with the sign convention of the spatial pattern as in Figure 6a is equated with a specific AOO regime as follows,

PSI PC1 > 0 corresponds to a cyclonic regime
(Proshutinsky Johnson AOO index < 0)

PSI PC1 < 0 corresponds to an anticyclonic regime
(Proshutinsky Johnson AOO index > 0).

[22] To justify our use of PSI PC1 to represent AOO, we run our model in a barotropic mode using exactly the same wind forcing. The resulting stream function variability has

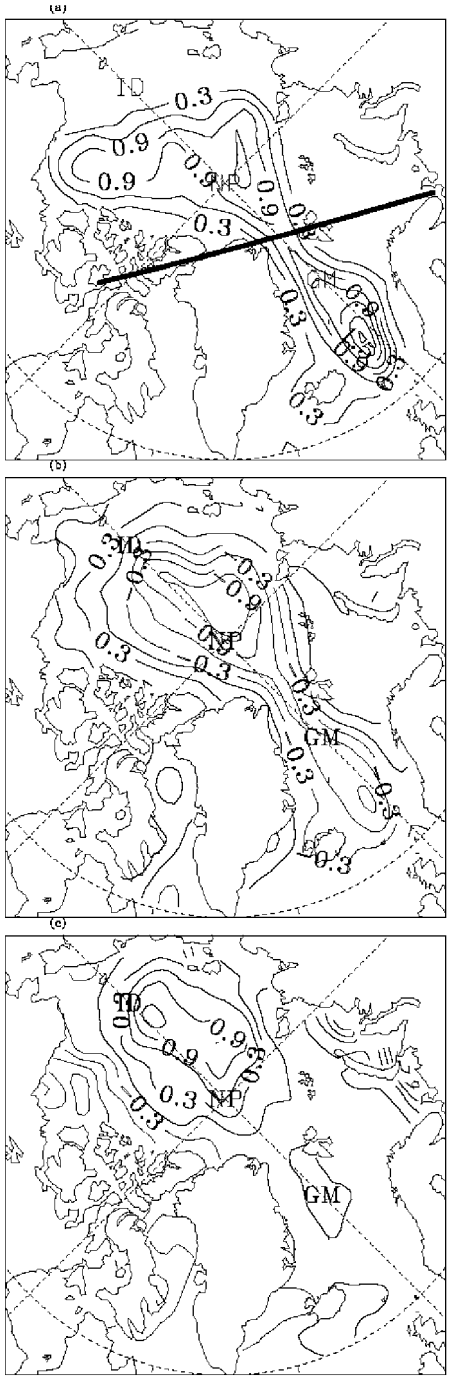

Figure 6. The first EOF modes of (a) vertical integrated transport stream function where positive contours correspond to cyclonic circulation, (b) sea surface height, and (c) the 100 m salinity. Thick and thin contours represent positive and negative values, respectively, with a contour interval of 0.3.

the first EOF mode undistinguishable from the spatial pattern in Figure 6a with further concentration onto the first mode (77.6%). The SSH EOF1 of the barotropic model has also similarity to Figure 6b, but with two (instead of one) centers of activity in the interior Arctic like in PSI EOF1. The cross correlations between PCs from the barotropic and the full model are shown in Table 1. In the barotropic case, the stream function and SSH PC1 in have a cross correlation of 0.98. Moreover, the stream function PCs from the two experiments are indistinguishable with correlation 0.94. The SSH PC1s from the two experiments are less strongly correlated, 0.68, as a manifestation of baroclinic effects in the full model SSH variability. In summary, we have a good reason to use the full model stream function PC1 to represent (negative of) AOO. Also, one can infer from the barotropic model results that wind forcing must be driving the first circulation mode. Since AO represents the largest portion of the variability in the atmosphere, the leading oceanic circulation mode has to be related to AO. The Arctic Ocean response is carried out through varying speed topographic waves, hence not all atmospheric variations have a simultaneous and uniformly distributed response in the ocean. Thus one cannot expect a perfect correlation between AO and PSI PC1.

[23] As shown above the SSH from a fully three-dimensional model includes also variations from the internal stratification changes, so the same AOO index is not exactly reproduced. The spatial pattern of the first SSH mode (with 26.2% of the variance) are shown in Figure 6b. The SSH EOF1 produces a pattern where the same SSH amplitude isolines are found circling the entire region north of the Nordic Sills. EOF patterns of Figures 6a–6b are quite similar to the ones found by *Häkkinen and Geiger* [2000] (although that study used a different surface forcing climatology and anomalies). Contrary to the unison behavior of PSI and SSH EOF1 over the Arctic, the first mode of the upper 100 m salinity (with 27.4% of the variance) has a spatial pattern as displayed in Figure 6c where the Siberian and Canadian Archipelago sides vary out of phase. This pattern is familiar from the correlations in Figure 4 which prominently describe the see-saw behavior of the salinity anomalies between the two sides of the Arctic Ocean. The various choices of the depth averaged salinity from 200 to 1000 m produces very similar pattern (but with diminishing amplitude) and PC1 as shown for the 100 m salinity.

[24] The first principal components of the stream function, SSH and 100 m salinity and the AO index (from the NOAA-CPC/NCEP tables) are shown in Figure 7 where each time series is binned into annual averages, linearly detrended and smoothed once with one binomial filter. (The modes shown for SSH and PSI are the first modes whether linear trend is removed before EOF analysis or not [*Häkkinen and Geiger*, 2000]). All quantities share similar behavior of maxima and minima with salinity PC1 slightly lagging the extrema of the other time series. The PSI PC1 is highly correlated (0.66 for annually averaged values) with AO. SSH and PSI PC1 correlate highly (0.74) but SSH PC1 has a weaker correlation (0.44) with AO because SSH PC1 lacks in amplitude like in the case of the 1962–1964 and 1982–1984 peaks. The lack of amplitude during these two events makes the SSH PC1 time series to appear having longer than decadal variability. The 100 m (200 m) salinity PC1 has correlations of 0.67 (0.62) with PSI PC1 and 0.48 (0.47) with AO when the PSI PC1 and AO lead by 1 year. These correlations are in Table 1.

[25] The effect of the anticyclonic and cyclonic regimes, as measured by PSI PC1, on the surface and depth averaged velocity (for 100 and 500 m) fields are shown in

Table 1. Correlations Between Annual Average Values of AO, PSI PC1 (=−AOO), SSH PC1 and S100 PC1 (Full Model), and PSI PC1 and SSH PC1 (Referenced With b) From a Barotropic Model (All Linearly Detrended)

	AO	PSI PC1	SSH PC1	S100 PC1	PSI PC1(b)	SSH PC1(b)
AO	1	0.66	0.44	0.48 (lag = 1yr)	0.71	0.69
PSI PC1	0.66	1	0.74	0.67 (lag = 1yr)	0.94	0.91
PSI PC1(b)	0.71	0.94	0.71	0.65(lag = 1yr)	1	0.98
SSH PC1	0.44	0.74	1	0.82	0.71	0.68

Figures 8a–8c as a correlation map. All fields have nonsignificant correlations at the center of the Canada Basin, but in each case the correlations reach maximum (over 0.8) off the East Siberian Sea and off the Canadian Archipelago. Figure 8 shows that the surface (and at least down to 100 m) anomalies tend to circulate in the Arctic as a response to AOO. Inclusion of deeper layer down to 500 m displays the significant effect of the Fram Strait exchange and the nearly continuous track of the Atlantic water and its mixed products around the whole Arctic Basin.

4.3. Source of Salinity/Freshwater Anomalies

4.3.1. Role of Gyre Dynamics; Testing the Hypothesis

[26] The basin average quantities of salt content and ice volume anomalies appear to have a weak common denominator both in time and in spatial distribution. The hypothesis put forward by *Proshutinsky et al.* [2002] suggests that the Beaufort Sea is the source of the freshwater anomalies which are created in the center of the anticyclonic Canada Basin gyre from the changes in the Ekman pumping. To investigate the importance of this dynamical effect we use a case study for the two most recent maximum and minimum anomalies. We chose years 1994 and 1986, which belong to cyclonic and anticyclonic regimes respectively. It should be noted that these two years also represent a year before and a year at the height of the 'Arctic warming' event [*Carmack et al.*, 1995].

[27] First we show the salinity fields averaged over 500 m and their difference in Figures 9a–9c. In 1994 the 34.0 and 34.2 ppt isohalines have invaded all the way to the Chuckhi Plateau and across the Lomonosov Ridge, while 1986 the same isohalines have a very limited reach to the Canada Basin. To compare the salinity anomaly field to the 'dynamic' anomaly field we show the depth of 34.5 ppt isohaline in 1994 and 1986 and the difference in Figures 10a–10c. As the hypothesis suggests the gyre is deeper by 30 m and expanded during the 1986 anticyclonic regime year compared to the 1994 cyclonic regime year. The largest depth anomalies are located in the easternmost part of the Canada Basin extending to the Eurasia Basin. To compare the differences in the Beaufort Gyre between the two years, we compute the area and volume where the 34.5 ppt isohaline is deeper than 360 m. We also compute the area average salinity in the upper 500 m in the area defined by the 360 m isobath (too cumbersome to limit to the actual volume enclosed by the 360 m and deeper isobaths). These computations give

1994 cyclonic area = 1.95E6 km2

volume = 7.94E5 km^3 salinity = 32.83 ppt

1986 anticyclonic area = 1.80E6 km2

volume = 7.43E5 km^3 salinity = 32.88 ppt

Some relaxation (about 10%) of the gyre in the 1994 cyclonic regime is detectable in the increased gyre area

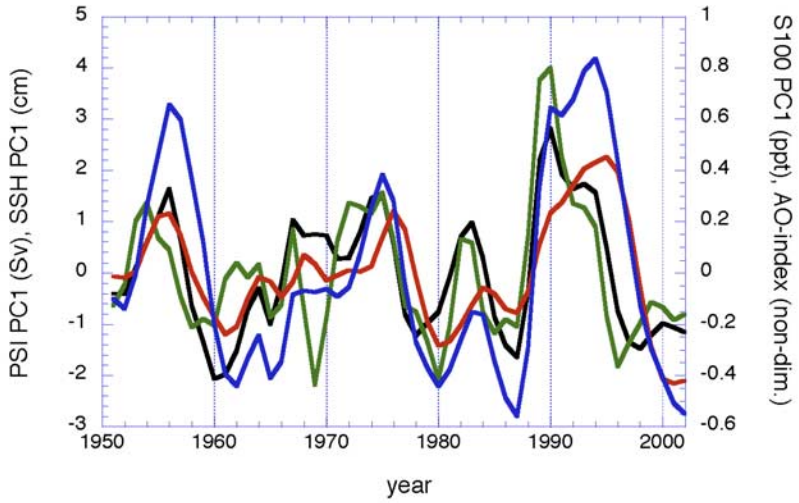

Figure 7. The principal component of the first mode for stream function (black), SSH (blue), 100 m salinity (red), and AO index (green). One binomial filter has been used to smooth the time series.

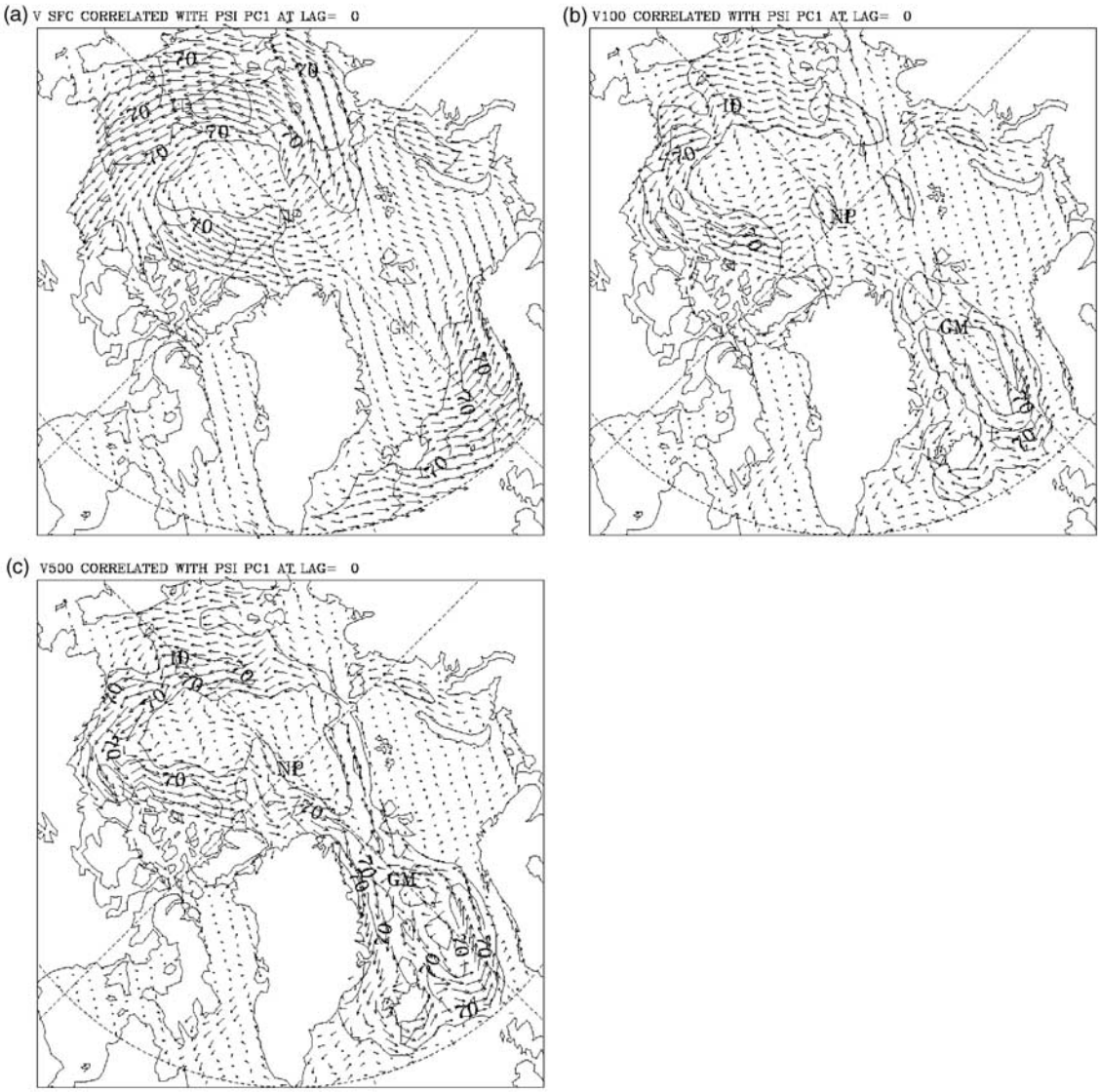

Figure 8. The correlation of PSI PC1 and the velocity fields (a) at surface, (b) in the top 100 m, and (c) in the top 500 m. The correlations are expressed as vectors from the individual u and v component correlations.

compared to the 1986 anticyclonic regime. The volume also increased slightly (6%) for the cyclonic regime, but the volume average salinity in the area defined by the 360 m isobath increased for the anticyclonic regime. In our case study we would have to add about 5000 km^3 of fresh water to the 1986 gyre to bring it to the salinity and volume in 1994. This should be compared to Figure 2 which shows that about a loss of about 6000 km^3 of fresh water took place from 1986 to 1994. Thus the changes in the depth and location of the Beaufort gyre do not determine the basin-scale freshwater anomaly. While we cannot claim that our case study is a definitive proof, we suggest that the Beaufort gyre contraction and relaxation process is present simply from the dynamical principles, but may not be the dominating effect in the basin-scale freshwater content changes. Also another problem for the hypothesis of the gyre relaxation and contraction is that it cannot address the strongly negative part of the salinity anomaly filed in Figure 6c.

[28] Previously the discussion of the principal components of the leading modes of variability has established the relationship between AOO regimes and the salinity PC1. In Figures 11a–11b we have a composite formed from the 500 m average salinity fields subtracting fields corresponding to anticyclonic (PSI PC1 <0) regimes from the fields corresponding to cyclonic (PSI PC1 >0) regimes when PSI PC1 amplitude exceeds one standard deviation. The largest salinity anomalies lag PSI PC1 by one year and follow closely the path of the Atlantic Waters depicted in the correlation maps in Figure 8. Again there is no indication that the largest anomalies would be at any time located atop of the center of the 34.5 ppt isohaline (Figures 10a–10b) used to define the bowl-like Beaufort Gyre. On the contrary the salinity anomalies appear to skirt the boundaries of

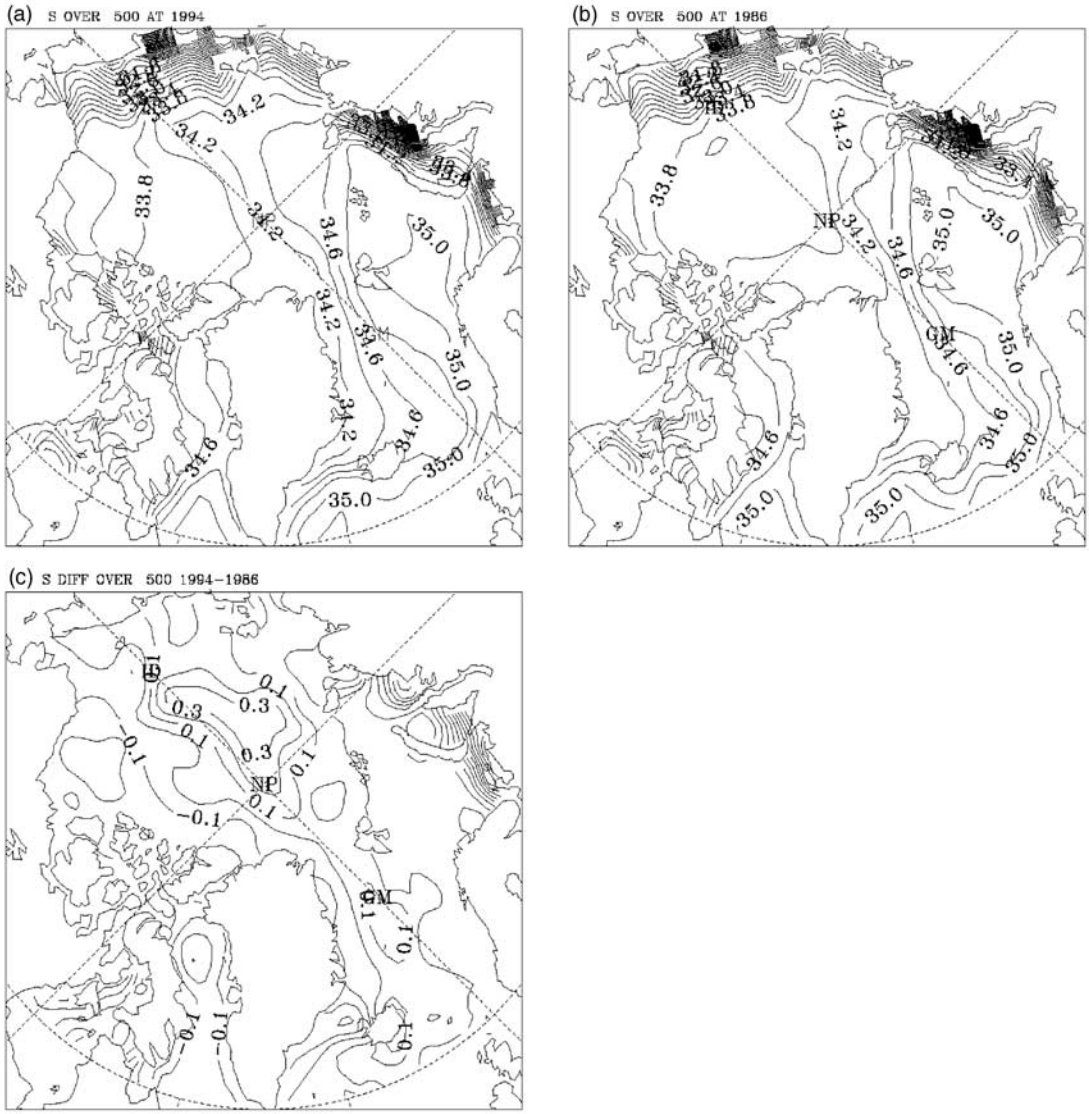

Figure 9. The salinity in the top 500 m (a) in 1994 (a cyclonic regime year) and (b) in 1986 (an anticyclonic regime year) and (c) their difference. Units are in ppt.

the gyre center following the current changes that are co-located in the same area (Figure 8).

[29] The creation of the salinity spatial anomaly field needs further evaluation, especially the anomaly center along the Alaskan-Canadian Coast. We form composites of salinity anomalies at 200 m depth (which cuts through the middle of the gyre depth) during cyclonic and anticyclonic regimes which should provide a good planar view of the subsurface Beaufort gyre and its location during the two circulation regimes. Figures 12a–12b (at lag 0, but lag = 1 fields are very similar and not shown) imply that there is a clear shift (more apparent than in Figure 10) in the location of the Beaufort Gyre when focusing on the minimum plotted isoline of 33.8 ppt: In the anticyclonic regime the gyre extends further toward the Siberian side than during the cyclonic regimes. During cyclonic regimes the gyre is pushed against the Alaskan-Canadian coast bringing fresher waters toward the coast. Thus the displacement of the gyre is the underlying cause to why the salinity anomaly field in Figure 12c emerges between the two circulation regimes.

4.3.2. Role of Sea Ice Growth and Melt

[30] Figure 4 gives a strong impression that the salinity anomalies are initiated at East-Siberian-Laptev Seas with opposing sign anomalies in the coastal Beaufort Sea. As noted earlier the influence of the positive AO is manifested as an offshore sea ice transport on the Siberian side which creates open water and thus more wintertime ice production. On the Canadian Archipelago side the positive AO associated ice drift packs the ice field against the coast removing any open water that would normally exist. To elucidate the resulting ice growth and melt (simulated) anomalies, an ice growth composite is formed on the basis of the AO index, so that first the growth fields at the AO index values exceeding one standard deviation, are binned corresponding to the negative and positive AO index values. Next, the fields corresponding to the negative index values are subtracted from those corresponding to the positive index

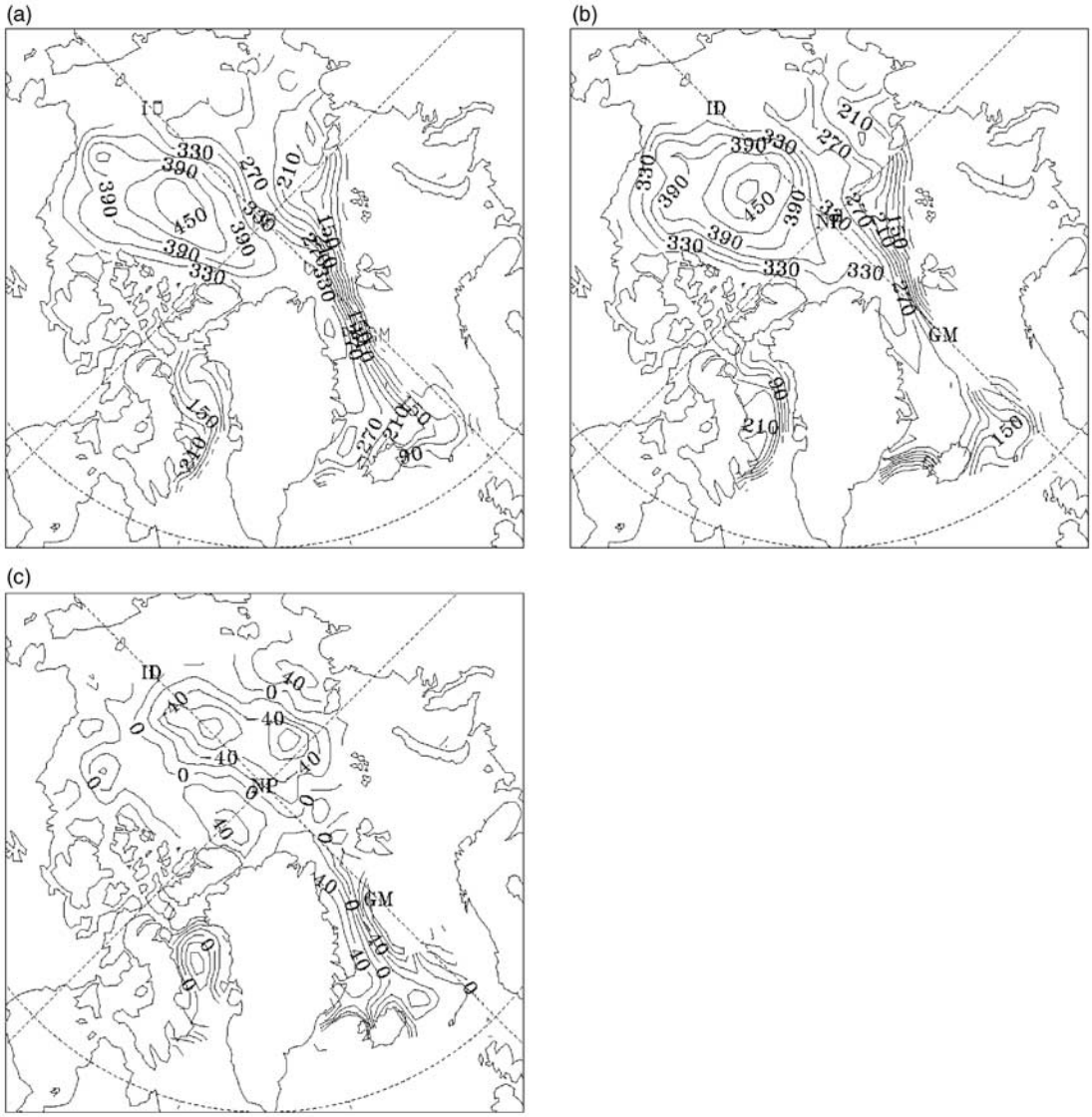

Figure 10. The depth of the 34.5 ppt isohaline (a) in 1994 and (b) in 1986 and (c) their difference. Depths are in meters.

values resulting into a difference field pictured in Figure 13a. The increased thermodynamic ice growth on the Siberian side and the decreased growth in the coastal Beaufort Sea have a direct influence on the upper ocean salinities. The interannual peak to peak variability reaches over 0.5 m of ice per year and since these positive and negative phases of AO can last for several years, the net ice growth/melt can reach 1 7m during one phase of AO. (Note: The anomalies in the marginal ice zones, in the GIN Seas and Labrador Sea, represent anomalies in ice melt, and not in ice growth.)

[31] To compare the salinity anomalies caused by the surface flux, as an example the East Siberian annual ice growth anomaly is matched against the freshwater content anomaly in the top 100 m of the same area in Figure 13b. The magnitudes of the freshwater equivalent in both quantities are of the same order, although the ice production may at times lack in the amplitude like around 1980. However, Figure 13b times series represent only a small fraction of the total freshwater anomaly depicted in Figure 2, and additionally it has to compete with the opposite sign contribution from the coastal Canadian Archipelago. Figure 13b shows also the net ice growth anomalies in the whole Arctic basin which is not of the same magnitude as the total (100 m) freshwater content anomalies. Often this quantity seems to out of phase with both of the East Siberian quantities especially in the latter half of the simulation. Thus net ice growth cannot explain the total freshwater content variations, but it appears to create and/or enhance the surface anomalies existing in the ocean at the both centers of the salinity dipole.

4.3.3. Role of Salt/Freshwater Exchange

[32] Now we have seen that the dynamics internal to the Arctic Ocean may not be dominating the freshwater balance, and neither is the coastal ice growth/melt large enough to explain the amplitude of freshwater content in Figure 2. Next we have to consider advection of salt in and out of the Arctic. The stream function variability described by the first EOF (with 72% of the variance) shows that most contours

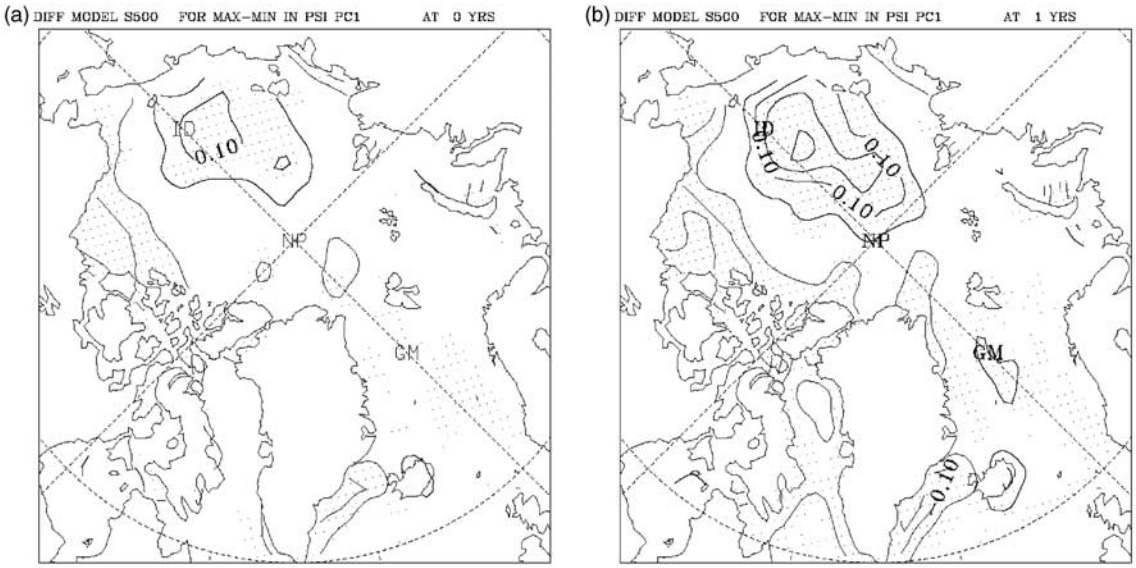

Figure 11. Composite of the upper 500 m salinity keyed to the PSI PC1 values larger than one standard deviation where fields corresponding to negative values of PSI PC1 are subtracted from the fields corresponding to positive values of PSI PC1. Composited 500 m salinity (a) at lag = 0 and (b) at lag = 1 year. The units are in ppt, and the dotted shading denote significance at 95% level.

in EOF1, equal or less than 0.8, are not closed within the Arctic but in the GIN Seas and beyond. There are 3 cells which close within the Arctic, one that covers the whole Arctic with contours values around 0.9, one weak subcell in the Canada Basin with maximum contour of 1.0 (not resolved in Figure 6a because of the contour interval), and another one in the Eurasia Basin with a contour range from 1.0 to 1.2. Thus exchange processes have to contribute significantly to variations in the freshwater/salt content in the main Arctic basin because close to 60% of the total transport variability within the Arctic is related to the inflow-outflow at the Fram Strait.

[33] The conservation of salt/fresh water is strongly controlled by advection of salt/fresh water, the surface flux contribution is minor compared to the advection through the boundaries [*Häkkinen*, 2002]. The mechanisms presented in section 3.1 and in this section could also be reframed to consider how the salt flux in these two cases would be registered at the boundary on the basis of the magnitude of the anomalies and the mean fields. If we define the salt flux in the outflowing (or inflowing) branch as $(S + s')(V + v')$, where S and V are the temporal mean salinity and transport and the primed quantities are anomalies from the mean. With these definitions the anomalous salt flux amounts to $(V + v')s' + v'S$. For simplicity we neglect the variations in the individual outlflow points along the boundary. A release of salinity/freshwater anomalies from the Beaufort Gyre would manifest through exchange terms such as $s'(V + v')$ (v' is similar in magnitude as V, the mean for the outflowing transports). This term can be compared with the remaining term of the anomalous salt flux, $v'S$, in the outflow branch. The values from the model simulations amount to comparison of ($\sim$3Sv $\times$ 34 ppt) versus ($\sim$3Sv $\times$ 0.5 ppt). On the basis of this the signal from the freshwater release would not register in the net effect on the freshwater storage of the Arctic, instead, the storage changes are dominated by transport anomalies acting on the (temporal) mean salinity field in either outflow or inflow branch. This dominance of transport anomalies is going to be shown next from the simulated data.

[34] Here the boundary for the Arctic freshwater content is chosen at the section transecting the Canadian Archipelago passages, the Fram Strait and the Barents Sea (Figure 6a) which was used as a boundary to compute the Arctic basin average quantities for freshwater and ice volume. We obtain the reference salinity from the average salinity over the 1000 m layer (Sa = 34.33 ppt), since it appears from Figure 2a that the anomalies saturate by 1000 m and assume that the deeper exchanges would give a net salt flux of zero. We are going to make estimates only on annual timescales, so any seasonal variability is neglected. We can formulate the freshwater balance as follows starting from the general salt conservation equation for the Arctic as a whole (here notation of Fram Strait is used for simplicity to refer to the boundary in the Atlantic sector inclusive of the Canadian Archipelago and Barents Sea):

$$Vol\ \delta S/\delta t = -\int v\ S\ dA\Big]_{\text{Bering}} + \int v\ S\ dA\Big]_{\text{Fram Strait}} - Qs - Qr, \tag{2}$$

where Qs and Qr are the surface (ice growth/melt + P − E) and river (virtual salt) volume fluxes, *Vol* is the volume of the Arctic, v is the velocity at the boundary, A the area of the boundary cross section. The first term on RHS and Qr do not contribute to freshwater anomalies (they are constant annually), and amount to a constant. Integration in time gives

$$Vol\ S(t) = \int \delta t\left\{\int v(x,z,t)S(x,z,t)dA\Big]_{\text{Fram Strait}} - Qs\right\} + \text{Constant}$$

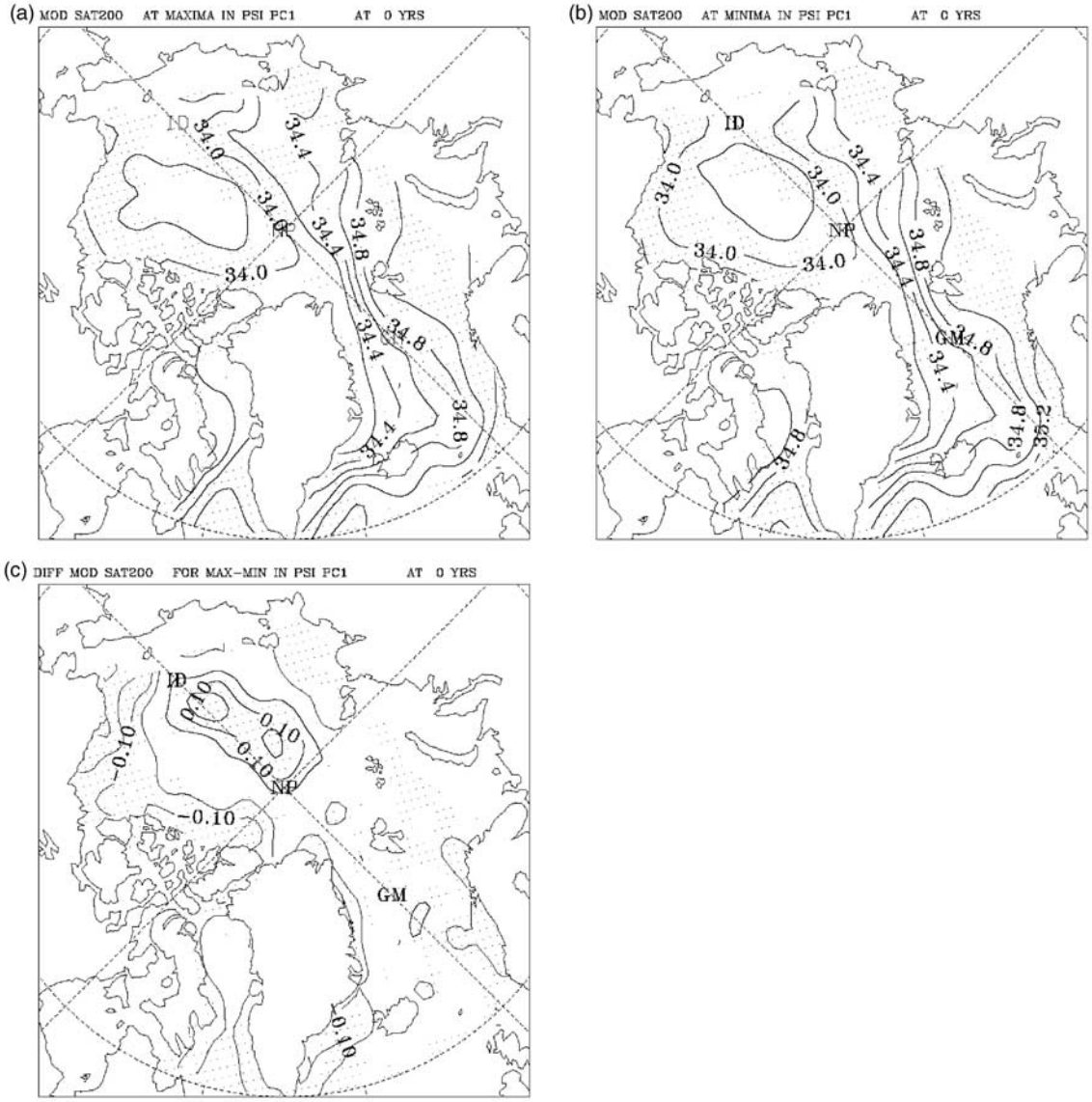

Figure 12. Composites of salinity at 200 m keyed to PSI PC1 and formed as in Figure 11. (a) The average field corresponding to the positive PSI PC1 (cyclonic regime) and (b) the corresponding to the negative PSI PC1 (anticyclonic regime). (c) The difference field. The units are in ppt, and shading shown in all figures denotes the significant areas of the difference at 95% level.

We can add terms involving constants like the basin average salinity (Sa) and divide both sides by Sa to be able to use formula (1), so we can write LHS to be the freshwater content anomaly FW(t) = *Vol* (Sa − S(t))/Sa. Removing any integration constants, and noting that only the ice growth/melt contributes (ice growth, Qsi, is negative freshwater input) to the time varying Qs, we arrive to anomalies:

$$\mathrm{FW}(t) = \int \delta t \left\{ \left[\int \mathrm{dA}\ v(x,z,t)\ (\mathrm{Sa} - S(x,z,t))/\mathrm{Sa} \right]_{\text{Fram Strait}} + \mathrm{Qsi}/\mathrm{Sa} \right\}$$

Using again formula (1), and noting that the term v(x, z, t)Sa in RHS is a constant on annual timescale and only the ice growth/melt contributes (ice growth, Qsi, corresponds to negative freshwater input) to the time varying part of Qs, we arrive to the anomalies

$$\mathrm{FW}\ (t) = \int \delta t \left\{ -\left[\int \mathrm{dA}\ v(x,z,t) S(x,z,t)/\mathrm{Sa} \right]_{\text{Fram Strait}} - \mathrm{Qsi}/\mathrm{Sa} \right\} \tag{3}$$

This equation is accurate up to this point, but in the following we apply approximations for v(x, z, t) and S(x, z, t). We choose the vertically averaged velocity anomaly to replace v(x, z, t) to emphasize the role of barotropic transport variations ($v'(x, t)$; nonseasonal monthly anomalies) at the boundary which are driven by large-scale wind field associated with AO. The other choice

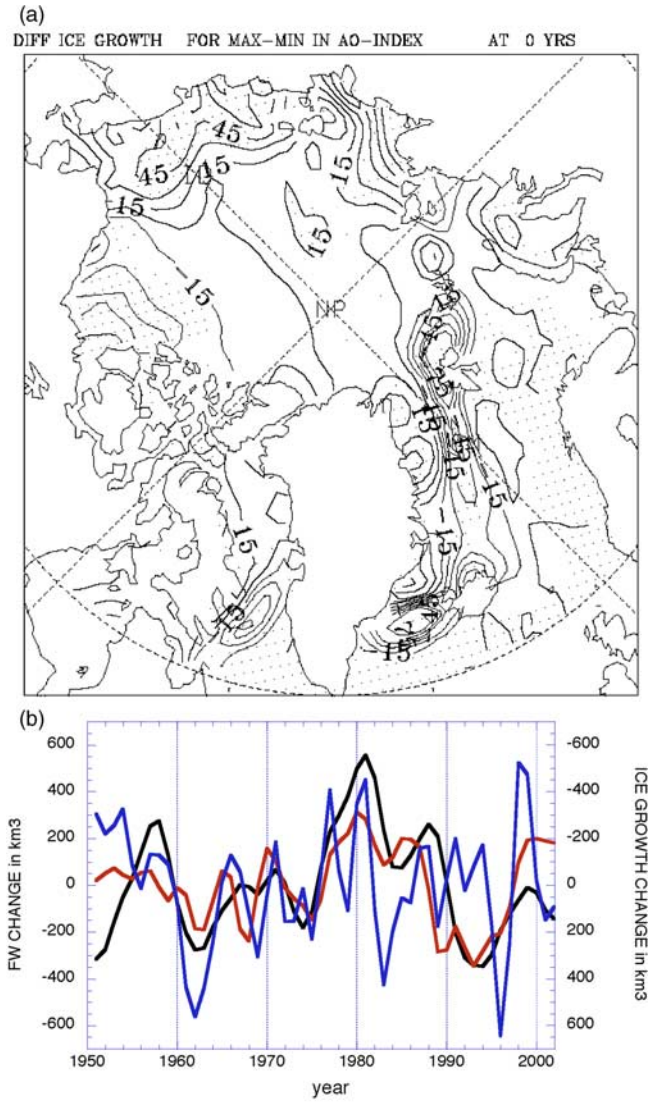

Figure 13. (a) Composite of the sea ice growth keyed to the AO index and formed as in Figure 11. The units are ice growth in cm/yr. Shading represents a significant difference at 95% level. (b) Ice growth volume anomaly in the East Siberian Sea (red) and in the whole Arctic (blue) and the freshwater content anomaly in the top (black) in the East Siberian Sea in units of km^3. One binomial filter has been used to smooth the time series.

is to emphasize the advection of mean salinity field by replacing S(x, z, t) by S(x, z); that is, there is no temporal variability in the salinity and no internal or external salinity anomalies are transported in or out. This yields:

$$FW(t) \sim \int \delta t \left\{ -\left[\int dx\, v'(x,t) \int dz\, S(x,z)/Sa \right]_{\text{Fram Strait}} - Qsi/Sa \right\} \quad (4)$$

After computation of RHS within the square brackets and ice growth anomaly values (removing any trends), the resulting values are added into cumulative sums to estimate the time integral. Figure 14 shows the cumulative sum derived from the first RHS term and from the cumulative sum of both RHS terms and for comparison, the freshwater anomaly in the top 1000 m computed directly from the salinity anomalies (in Figure 2a). Our approximation for the freshwater content changes on the basis of the barotropic mean flow changes acting on the mean salinity field at the boundary appears to estimate best the evolution of the basin freshwater storage. The inclusion of net ice growth anomalies improve the agreement slightly in the latter part of the simulation period although some of the ice growth related anomalies may exit the basin within one year.

[35] In summary, the net cumulative effect of the barotropic boundary transport changes alone gives an excellent fit and magnitude to match the basin freshwater storage anomalies. If there would have been a significant accumulation/release process internal to the Arctic, the amplitude of the freshwater content variability should differ considerably from the one predicted from the barotropic exchange at the

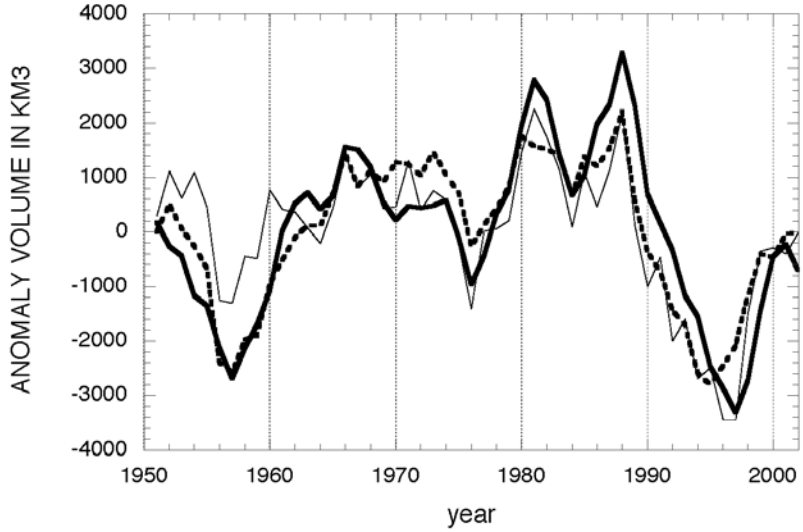

Figure 14. The Arctic freshwater anomaly in top 1000 m (same as in Figure 2a) (thick), the cumulative sum of freshwater anomaly (1) from the boundary exchange with the lower latitudes by the barotropic mean flow (dashed), (2) from barotropic mean flow and net ice growth anomalies, and freshwater anomaly due to ice growth (thin). All units are km^3.

Arctic 'boundary'. Also with the guidance from this exercise we can make an estimate of the changes from the omitted freshwater fluxes by accumulating the river flux, P-E and the estimated Bering inflow changes. The cumulative sum of the omitted flux values vary between +1400 and −900 km^3 (not shown), although not negligible, its amplitude falls short of the basin average variability from the anomalous advection.

5. Conclusions

[36] We have analyzed interannual variability of freshwater in the Arctic Ocean and sources of this variability on the basis of model simulation for the period 1951–2002. The model is a coupled ice-ocean model [*Häkkinen and Mellor*, 1992] covering the Arctic Ocean and Atlantic Ocean south to 16S. The coupled model is forced by NCEP/NCAR Reanalysis data after a spin-up phase of 26 years with 20 years using climatology computed from the Reanalysis data and 6 year transition phase to the start (1951) of the analyzed time series. River runoff, Bering Strait inflow and precipitation minus evaporation changes are not taken into account.

[37] Three major processes were considered to be responsible for variations in the Arctic freshwater storage. The first process to be considered was Ekman pumping in the Beaufort Gyre as a cause for the accumulation and release of freshwater depending whether the circulation regime is anticyclonic/cyclonic [*Proshutinsky et al.*, 2002]. We find that the effect of Ekman pumping is present but its impact on salinity distribution is not obvious. A factor contributing to the failure of the Ekman pumping related processes in the simulation is that the Beaufort Gyre in the model is very weak, and the stream function anomalies are strongly concentrated to a mode (over 70% of the variability) involving the whole basin and the GIN Seas. However, there are signals that the Arctic freshwater variability in general correlates with (AO and) AOO variations. One could point out that AOO clearly influences the location of the anticyclonic gyre in the Canada Basin shifting it further eastward for the anticyclonic regime and westward against the Alaskan-Canadian coast for the cyclonic regime.

[38] The second process with an obvious potential to change the freshwater content is the variability of sea ice growth and melt and it is shown that it is not very important except changes in salinity associated with ice growth and melt in the Siberian and Canadian sectors of Arctic. However, the sea ice growth/melt anomalies in the East Siberian Sea could be important for the downstream stratification because these anomalies appear to propagate rapidly to the Greenland Sea where they have potential to disrupt the water renewal processes.

[39] The third process to be considered was the exchange of water masses with the GIN Seas by the advection of Atlantic Waters to the Arctic Ocean. We find that this process explains most of variability in freshwater content in the top 1000 m in this model simulation. The most prominent signature of this process in the case of cyclonic regime is the intrusion of high-salinity waters to the Canada Basin which displace the Beaufort Gyre further westward. This process makes the positive salinity anomalies to appear offshore from the East Siberian Sea and negative anomalies (because the fresh waters of the gyre displaces the slightly more saline coastal waters) to appear at the southern rim of the Canada Basin along the Alaskan and Canadian Coasts. It happens that AO variability impacts also ice growth/melt in these areas, but the ice growth related anomalies are much smaller than the basin average anomalies. A word of caution concerning the dominating role of exchange of water masses is appropriate because the model strongly concentrates the stream function anomalies to a pattern which connects the Arctic Basin to the GIN Seas. Thus it is no surprise that the advective processes would be overriding any internal mechanisms.

[40] In summary we find that the exchange processes between Arctic Ocean and rest of the world oceans consti-

tute the largest impact on the freshwater content variability in the Arctic at least in the numerical model we used. The largest decrease in the simulated Arctic freshwater content, which started in the late 1980s and continued to the mid-1990s, coincides with the Arctic Atlantic layer warming [*Carmack et al.*, 1995]. During this event, the frontal structures were displaced nearly 1000 km farther west from the Lomonosov Ridge to the Mendeleyev Ridge [*Carmack et al.*, 1995]. Such shift is difficult explain without invoking a large change in the volume transport of the Atlantic waters, and this is the key component in this model to explain the freshwater storage anomalies in the Arctic.

[41] **Acknowledgments.** We thank L. Timokhov from the Arctic-Antarctic Institute for making available the Russian data. We thank Lena Marshak in helping to make possible highly efficient parallel code simulations. We gratefully acknowledge the support from National Science Foundation under Grant No OPP-0230184 (AP) and from NASA Headquarters (SH). This is contribution no 11012 of the Woods Hole Oceanographic Institution (AP).

References

Aagaard, K., and E. C. Carmack (1989), The role of sea ice and fresh water in the Arctic circulation, *J. Geophys. Res.*, *94*, 14,485–14,498.

Blumberg, A. F., and G. L. Mellor (1987), A description of a three-dimensional coastal ocean circulation model, in *Three Dimensional Coastal Ocean Models*, *Coastal Estuarine Sci.*, vol. 4, edited by N. S. Heaps, pp. 1–16, AGU, Washington, D. C.

Carmack, E. C., R. W. Macdonald, R. G. Perkin, F. A. McLaughlin, and R. J. Peterson (1995), Evidence of warming of Atlantic layer water in the southern Canada Basin of the Arctic Ocean, *Geophys. Res. Lett.*, *22*, 1061–1064.

Coachman, L. K., and K. Aagaard (1988), Transport through Bering Strait: Annual and interannual variability, *J. Geophys. Res.*, *93*, 15,535–15,539.

Coachman, L. K., K. Aagaard, and R. B. Tripp (1975), *Bering Strait: The Regional Physical Oceanography*, 172 pp., Univ. of Wash. Press, Seattle.

da Silva, A. M., C. C. Young, and S. Levitus (1994), *Atlas of Surface Marine Data 1994*, vol. 1, *Algorithms and Procedures, NOAA Atlas NESDIS*, vol. 6, 83 pp., Natl. Oceanic and Atmos. Admin., Silver Spring, Md.

Dickson, R. R., J. Meincke, S.-A. Malmberg, and A. J. Lee (1988), The "Great Salinity Anomaly" in the northern North Atlantic 1968–82, *Prog. Oceanogr.*, *20*, 103–151.

Dickson, R. R., J. Lazier, J. Meincke, P. Rhines, and J. Swift (1996), Long-term coordinated changes in the convective activity of the North Atlantic, *Prog. Oceanogr.*, *38*, 241–295.

Ekwurzel, B., P. Schlosser, R. A. Morlock, and R. G. Fairbanks (2001), River runoff, sea ice melt-water, and Pacific water distribution and man residence times in the Arctic Ocean, *J. Geophys. Res.*, *106*, 9075–9092.

Goosse, H., F. M. Selton, R. J. Haarma, and J. D. Opsteegh (2002), A mechanism of decadal variability of the sea ice volume in the Northern Hemisphere, *Clim. Dyn.*, *19*, 61–83.

Häkkinen, S. (1993), An Arctic source for the Great Salinity Anomaly: A simulation of the Arctic ice-ocean system for 1955–1975, *J. Geophys. Res.*, *98*, 16,397–16,410.

Häkkinen, S. (1999), Variability of the simulated meridional heat transport in the North Atlantic for the period 1951–1993, *J. Geophys. Res.*, *104*, 10,991–11,007.

Häkkinen, S. (2000), Decadal air-sea interaction in the North Atlantic based on observations and modeling results, *J. Clim.*, *13*, 1195–1219.

Häkkinen, S. (2001), Variability in sea surface height: A qualitative measure for the meridional overturning in the North Atlantic, *J. Geophys. Res.*, *106*, 13,837–13,848.

Häkkinen, S. (2002), Surface salinity variability in the northern North Atlantic during recent decades, *J. Geophys. Res.*, *107*(C12), 8003, doi:10.1029/2001JC001267.

Häkkinen, S., and C. A. Geiger (2000), Simulated low frequency modes of circulation in the Arctic Ocean, *J. Geophys. Res.*, *105*, 6549–6564.

Häkkinen, S., and G. L. Mellor (1992), Modeling the seasonal variability of the coupled Arctic ice-ocean system, *J. Geophys. Res.*, *97*, 20,285–20,304.

Hilmer, M., and P. Lemke (2001), On the decrease of Arctic sea ice volume, *Geophys. Res. Lett.*, *27*, 3751–3754.

Holland, M. M., C. M. Bitz, M. Eby, and A. J. Weaver (2001), The role of ice-ocean interactions in the variability of the North Atlantic thermohaline circulation, *J. Clim.*, *14*, 656–675.

Maslowski, W., B. Newton, P. Schlosser, A. Semtner, and D. Martinson (2000), Modeling recent climate variability in the Arctic Ocean, *Geophys. Res. Lett.*, *27*, 3743–3746.

Mauritzen, C., and S. Häkkinen (1997), Influence of the sea ice on the thermohaline circulation in the North Atlantic Ocean, *Geophys. Res. Lett.*, *24*, 3257–3260.

Mellor, G. L., and T. Yamada (1982), Development of a turbulence closure model for geophysical fluid problems, *Rev. Geophys.*, *20*, 851–875.

Polyakov, I. V., A. Y. Proshutinsky, and M. A. Johnson (1999), Seasonal cycles in two regimes of Arctic climate, *J. Geophys. Res.*, *104*, 25,761–25,788.

Proshutinsky, A. Y., and M. A. Johnson (1997), Two circulation regimes of the wind driven Arctic Ocean, *J. Geophys. Res.*, *102*, 12,493–12,514.

Proshutinsky, A., R. H. Bourke, and F. A. McLaughlin (2002), The role of the Beaufort Gyre in the Arctic climate variability: Seasonal to decadal climate scales, *Geophys. Res. Lett.*, *29*(23), 2100, doi:10.1029/2002GL015847.

Rigor, I. G., J. M. Wallace, and R. L. Colony (2002), Response of sea ice to the Arctic Oscillation, *J. Clim.*, *15*, 2648–2663.

Shiklomanov, I. A., A. I. Shiklomanov, R. B. Lammers, B. J. Peterson, and A. J. Vorosmarty (2000), The dynamics of river water inflow to the Arctic Ocean, in *Fresh Water budget of the Arctic Ocean*, edited by E. L. Lewis, pp. 281–296, Kluwer Acad., Norwell, Mass.

Thompson, D. W. J., and J. M. Wallace (1998), Observed linkages between Eurasian surface air temperature, the North Atlantic Oscillation, Arctic sea level pressure and the stratospheric polar vortex, *Geophys. Res. Lett.*, *25*, 1297–1300.

Vinje, T. (2001), Fram Strait ice fluxes and atmospheric circulation 1950–2000, *J. Clim.*, *14*, 3508–3517.

Walsh, J. E., W. D. Hibler, and B. Ross (1985), Numerical simulation of Northern Hemisphere sea ice variability, 1951–1980, *J. Geophys. Res.*, *90*, 4847–4865.

S. Häkkinen, NASA Goddard Space Flight Center, Code 971, Greenbelt, MD 20771, USA. (sirpa.hakkinen@nasa.gov)

A. Proshutinsky, WHOI, MS 29, 360 Woods Hole Rd, Woods Hole, MA 02543, USA.